Available online at www.sciencedirect.com
SCIENCE DIRECT®
Journal of Catalysis 231 (2005) 300–313
JOURNAL OF CATALYSIS
www.elsevier.com/locate/jcat

Thiophene hydrodesulfurization over nickel phosphide catalysts: effect of the precursor composition and support

Stephanie J. Sawhill [a], Kathryn A. Layman [a], Daniel R. Van Wyk [a], Mark H. Engelhard [b], Chongmin Wang [b], Mark E. Bussell [a,*]

[a] *Department of Chemistry, MS-9150, Western Washington University, 516 High Street, Bellingham, WA 98225, USA*
[b] *Environmental Molecular Sciences Laboratory, Pacific Northwest National Laboratory, P.O. Box 999, K8-93, Richland, WA 99352, USA*

Received 30 September 2004; revised 6 January 2005; accepted 12 January 2005

Available online 17 March 2005

Abstract

Silica- and alumina-supported nickel phosphide (Ni_xP_y) catalysts have been prepared, characterized by bulk and surface sensitive techniques, and evaluated for the hydrodesulfurization (HDS) of thiophene. Series of 30 wt% Ni_xP_y/SiO_2 and 20 wt% Ni_xP_y/Al_2O_3 catalysts were prepared from oxidic precursors with a range of P/Ni molar ratios by temperature-programmed reduction (TPR) in flowing H_2. Oxidic precursors with molar ratios of P/Ni = 0.8 and 2.0 yielded catalysts containing phase-pure Ni_2P on the silica and alumina supports, respectively. At lower P/Ni ratios, significant $Ni_{12}P_5$ impurities were present in the Ni_xP_y/SiO_2 and Ni_xP_y/Al_2O_3 catalysts as indicated by X-ray diffraction. The HDS activities of the Ni_xP_y/SiO_2 and Ni_xP_y/Al_2O_3 catalysts depended strongly on the P/Ni molar ratio of the oxidic precursors with optimal activities obtained for catalysts containing phase-pure Ni_2P and minimal excess P. After 48 h on stream, a Ni_2P/SiO_2 catalyst was 20 and 3.3 times more active than sulfided Ni/SiO_2 and $Ni–Mo/SiO_2$ catalysts, respectively. A Ni_2P/Al_2O_3 catalyst was 2.7 times more active than a sulfided Ni/Al_2O_3 catalyst but only about half as active as a sulfided $Ni–Mo/Al_2O_3$ catalyst.

Keywords: Nickel phosphide; Hydrotreating; Hydrodesulfurization; HDS; Thiophene

1. Introduction

A new class of materials, the transition-metal phosphides (e.g., MoP [1–3], WP [3–5], and Ni_2P [6–17]), have recently been the focus of research within the catalysis community, as these materials have shown high hydrodesulfurization (HDS) and hydrodenitrogenation (HDN) activity. It is hoped, therefore, that the development of metal phosphide-based hydrotreating catalysts may help to meet future environmental regulations requiring significant reductions in the allowable sulfur levels in transportation fuels.

In a previous study, we described the HDS catalytic properties of Ni_2P/SiO_2 catalysts with a wide range of loadings and compared them with sulfided Ni/SiO_2, Mo/SiO_2, and $Ni–Mo/SiO_2$ (Ni/Mo = 0.5) catalysts [13]. Briefly, we observed that the thiophene HDS activity, after 100 h on stream, of a 30 wt% Ni_2P/SiO_2 catalyst was approximately 15 and 3 times more active than sulfided Mo/SiO_2 and $Ni–Mo/SiO_2$ catalysts, respectively. In addition, silica-supported Ni_2P catalysts showed excellent stability under HDS conditions. The HDS activities of Ni_2P/SiO_2 catalysts correlated with their O_2 chemisorption capacities, and it was concluded that the high HDS activity of Ni_2P/SiO_2 catalysts can be traced to both a high site density and a high turnover frequency (TOF).

Research in a number of laboratories has shown that the TPR synthesis of phase-pure Ni_2P on silica requires the use of excess P in the oxidic precursor [3,7,8,12,13,15]. Time-resolved X-ray diffraction (XRD) investigation of the TPR synthesis of a Ni_2P/SiO_2 catalyst revealed that reduction of an oxidic precursor with P/Ni = 0.8 proceeded sequentially,

* Corresponding author. Fax: 360-650-2826.
E-mail address: mark.bussell@wwu.edu (M.E. Bussell).

0021-9517/$ – see front matter
doi:10.1016/j.jcat.2005.01.020

with silica-supported NiO converted first to Ni metal, then to $Ni_{12}P_5$, and finally to Ni_2P [12]. Oyama and co-workers [8,15] showed that some excess P is volatilized during TPR as PH_3, and that some of the additional excess P remains associated with the silica support.

Since a number of studies have reported that the preparation and hydrotreating properties of Ni_2P/SiO_2 catalysts are sensitive to the precursor composition [7,8,13–15], we have investigated in detail the effect of precursor composition on the HDS properties of silica-supported Ni_xP_y catalysts. Furthermore, since the typical support for commercial hydrotreating catalysts is γ-Al_2O_3, we have carried out a parallel investigation of Ni_xP_y/Al_2O_3 catalysts. Alumina interacts more strongly with phosphorus than does silica, and this interaction is expected to influence the catalytic properties of the supported Ni phosphides.

2. Experimental

2.1. Catalyst preparation

2.1.1. Ni_xP_y/SiO_2

Catalysts containing 30 wt% Ni_xP_y/SiO_2 were prepared from oxidic precursors with molar ratios of P/Ni = 0.4, 0.5, 0.8, 1.0, 1.5, and 2.0, by a procedure described in detail elsewhere [13]. This weight loading was determined to be optimal for thiophene HDS as reported previously [13]. 20 wt% $Ni_{12}P_5/SiO_2$ and Ni_2P/SiO_2 catalysts, used for the IR spectroscopic measurements, were prepared from oxidic precursors with P/Ni = 0.4 and 0.8, respectively, by a similar procedure.

2.1.2. Ni_xP_y/Al_2O_3

Catalysts containing 20 wt% Ni_xP_y/Al_2O_3 were prepared from oxidic precursors with molar ratios of P/Ni = 0.5, 0.8, 1.0, 1.5, 2.0, and 2.5. This weight loading was selected because of the lower surface area of the alumina support (compared with the silica) and because a 20 wt% Ni_2P/Al_2O_3 catalyst had a higher activity than a catalyst with a 30 wt% loading. The γ-Al_2O_3 (Degussa; Aluminum Oxide C, 100 m^2/g) was calcined at 773 K before use and was impregnated with an aqueous solution of $Ni(NO_3)_2 \cdot 6H_2O$ (Alfa Aesar; 99.9985%) and $NH_4H_2PO_4$ (Baker; 99.1%) to give the desired P/Ni molar ratio in the catalyst precursor. The precursors were dried at 393 K and calcined in air at 773 K for 3 h. The TPR procedure was similar to that described elsewhere for Ni_2P/SiO_2 catalysts [13], except that the maximum temperature reached was 1123 K instead of 923 K.

2.1.3. SiO_2- and Al_2O_3-supported NiO, MoO_3, and NiO–MoO_3

Oxidic precursors of silica- and alumina-supported sulfided Ni, Mo, and Ni–Mo (Ni/Mo = 0.5) catalysts were prepared as described elsewhere [2,13].

2.2. Catalyst characterization

The catalysts prepared in this study were characterized by elemental analysis, BET surface area and O_2 chemisorption measurements, X-ray diffraction (XRD), X-ray photoelectron spectroscopy (XPS), transmission electron microscopy (TEM), and infrared (IR) spectroscopy. The details of the BET surface area, O_2 chemisorption, XRD, and XPS measurements have been described elsewhere [13,18].

Analysis of the Ni and P contents of Ni_xP_y/SiO_2 and Ni_xP_y/Al_2O_3 catalysts was carried out by Huffman Laboratories, Inc. The S content of Ni_xP_y/SiO_2 and Ni_xP_y/Al_2O_3 catalysts subjected to H_2S/H_2 pretreatments was determined with a LECO SC-144DR Sulfur and Carbon Analyzer. After degassing in flowing He at room temperature, the catalysts were heated to 650 K in 1 h and maintained at 650 K for 2 h, while under a 60 ml/min flow of a 3.03 mol% H_2S/H_2 mixture. The samples were subsequently flushed with He (60 ml/min) for 30 min at room temperature and then passivated for 2 h under a 60 ml/min flow of a 1 mol% O_2/He mixture. Approximately 0.3 g of catalyst was loaded into the LECO analyzer, where it was combusted in pure O_2 at 1623 K, and SO_2 in the effluent was quantified with an IR detector.

The vacuum system used for IR spectroscopic measurements and the sample mounting procedure have been described in detail elsewhere [19]. Transmission FTIR spectra were acquired over the 4000–1000 cm^{-1} range (128 scans, 4 cm^{-1} resolution) with procedures described elsewhere [16]. After mounting, the catalyst samples were evacuated to 10^{-3} Torr over a period of $\sim$ 30 min before reduction in flowing H_2 (60 sccm) at 650 K for 1 h. The samples were subsequently evacuated to $\sim 1 \times 10^{-7}$ Torr, annealed at 650 K for 1 min, and cooled to room temperature, and a background IR spectrum was acquired. An IR spectrum of adsorbed CO was then collected at 298 K while the catalyst sample was in the presence of 5.0 Torr CO. IR spectra were collected for silica- and alumina-supported Ni_2P, $Ni_{12}P_5$, and Ni catalysts, all with 20 wt% loadings.

2.3. Thiophene HDS activity measurements

Thiophene HDS activity measurements were carried out at 643 K with a feed consisting of a 3.2 mol% thiophene/H_2 mixture as described elsewhere [13,16]. The Ni_xP_y/SiO_2 and Ni_xP_y/Al_2O_3 catalysts were pretreated by degassing in He (60 ml/min) at room temperature for 30 min, and the SiO_2- and Al_2O_3-supported NiO, MoO_3, and NiO–MoO_3 catalysts were sulfided as described elsewhere [13]. Thiophene HDS activities ($nmol_{Th}/(g_{cat}\,s)$) were calculated from the total product peak areas calculated from the chromatogram after 48 h of reaction time.

Table 1
Physiochemical data for silica-supported Ni_2P catalysts

Oxidic precursor molar ratio (P/Ni)	XRD phase(s)	Bulk composition	Surface composition	BET surface area (m^2/g)	Chemisorption capacity ($\mu mol_{O_2}/g$)	HDS activity[a] ($nmol_{Th}/(g_{cat}\ s)$)	HDS TOF[a] (s^{-1})
0.40	$Ni_{12}P_5$	$Ni_{2.46}P_{1.00}$	$Ni_{3.88}P_{1.00}$	105	214	693	0.0032
0.50	$Ni_{12}P_5$, Ni_2P	$Ni_{1.88}P_{1.00}$	–	90	144	1970	0.014
0.80	Ni_2P	$Ni_{1.64}P_{1.00}$	$Ni_{2.23}P_{1.00}$	79	130	2750	0.021
1.0	Ni_2P	$Ni_{1.33}P_{1.00}$	–	79	76	2130	0.028
1.5	Ni_2P	$Ni_{0.89}P_{1.00}$	–	51	19	805	0.043
2.0	Ni_2P	$Ni_{0.58}P_{1.00}$	–	36	12	575	0.048

[a] After 48 h on-stream.

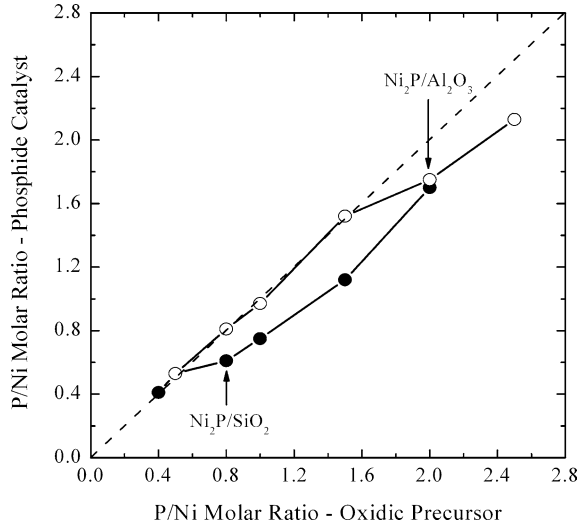

Fig. 1. A plot of the P/Ni molar ratio of Ni_xP_y/SiO_2 and Ni_xP_y/Al_2O_3 catalysts as a function of the P/Ni molar ratio of their oxidic precursors.

3. Results

3.1. Catalyst characterization

3.1.1. Elemental analysis, X-ray diffraction, and transmission electron microscopy

The elemental compositions of the Ni_xP_y/SiO_2 catalysts are listed in Table 1, and the P/Ni molar ratios of the oxidic precursors and the Ni_xP_y/SiO_2 catalysts are plotted against one another in Fig. 1. For Ni_xP_y/SiO_2 catalysts prepared from oxidic precursors with P/Ni > 0.5, some P is lost from the catalysts during TPR, but, except for the catalyst with P/Ni = 0.4, the catalysts contain P in excess of that expected from the stoichiometry of Ni_2P. XRD patterns for the Ni_xP_y/SiO_2 catalysts and for unsupported Ni_2P, as well as a JCPDS reference pattern for $Ni_{12}P_5$ (card no. 22-1190 [20]), are shown in Fig. 2. The XRD pattern of the unsupported Ni_2P is similar to a reference pattern from the JCPDS powder diffraction file (card no. 089-2742 [20]). The XRD pattern for the Ni_xP_y/SiO_2 catalyst with a molar ratio P/Ni = 0.4 in the oxidic precursor shows only the peaks observed in the $Ni_{12}P_5$ reference pattern. Henceforth, this catalyst (P/Ni = 0.4) will be referred to as $Ni_{12}P_5/SiO_2$. The elemental composition of the $Ni_{12}P_5/SiO_2$ catalyst was determined to

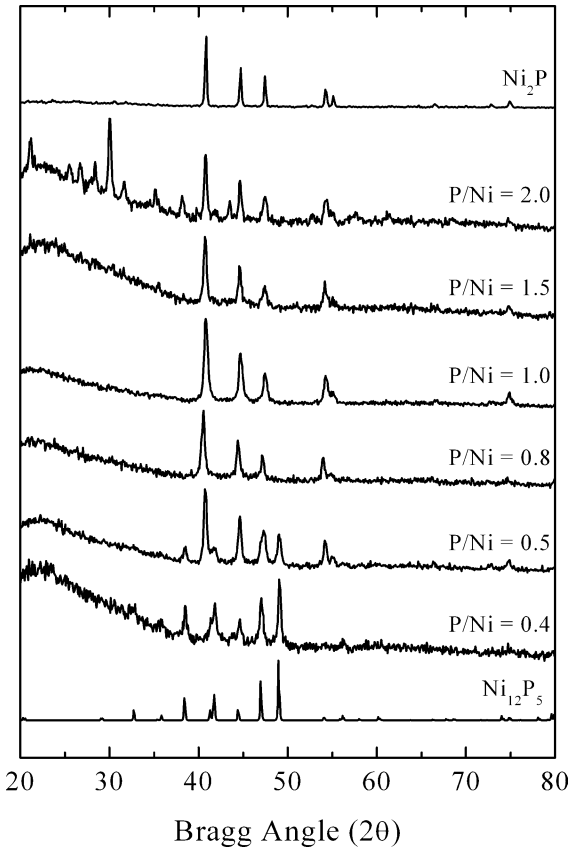

Fig. 2. XRD patterns for Ni_xP_y/SiO_2 catalysts with different P/Ni molar ratios in their oxidic precursors.

be $Ni_{2.46}P_{1.00}$, which is in good agreement with the expected stoichiometry ($Ni_{2.4}P_{1.0}$). As the amount of phosphorus in the oxidic precursor is increased to a molar ratio P/Ni = 0.5, the XRD pattern exhibits peaks for both $Ni_{12}P_5$ and Ni_2P. Phase-pure Ni_2P is achieved for the Ni_xP_y/SiO_2 catalyst prepared from an oxidic precursor with a molar ratio P/Ni ratio = 0.8. Henceforth, this catalyst (P/Ni = 0.8) will be referred to as Ni_2P/SiO_2. The elemental composition of the Ni_2P/SiO_2 catalyst was determined to be $Ni_{1.64}P_{1.00}$, which is quite P-rich compared with the composition expected from the stoichiometry of Ni_2P. As the molar ratio in the oxidic precursors is increased further (P/Ni > 0.8), Ni_2P is the only crystalline phase observed in the XRD patterns of the Ni_xP_y/SiO_2 catalysts up to a molar ratio of P/Ni = 2.0.

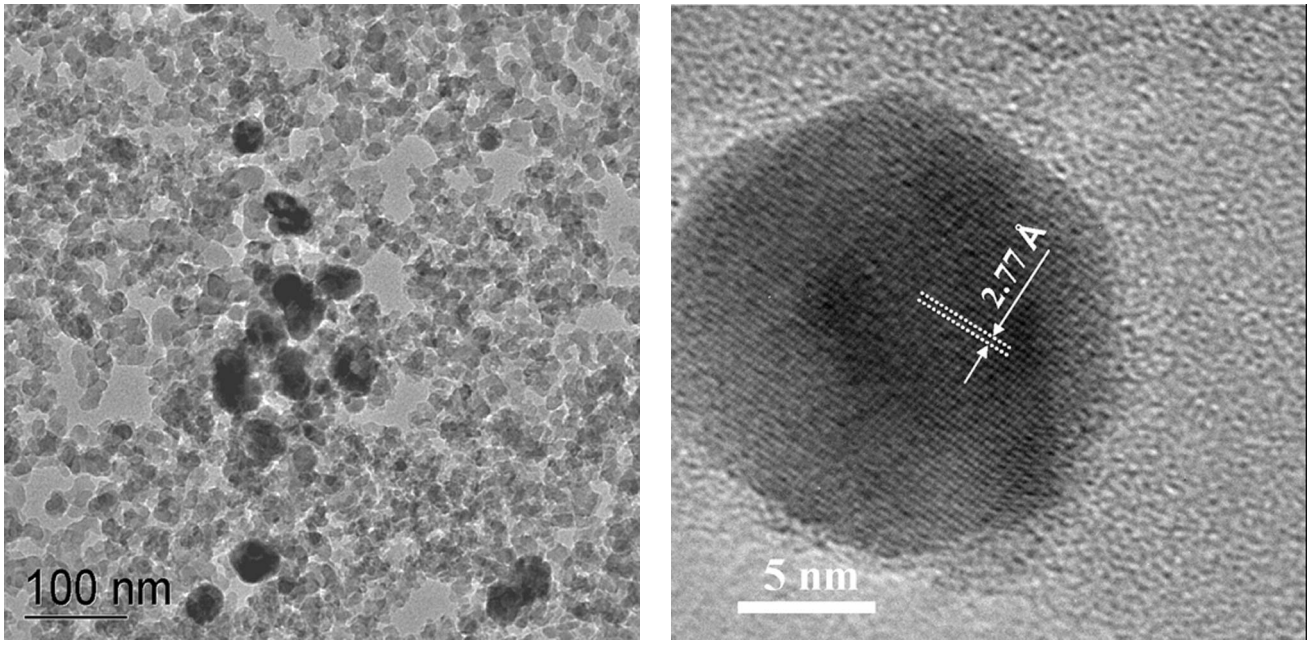

(a) (b)

Fig. 3. (a) Low and (b) high resolution TEM micrographs of a 30 wt% $Ni_{12}P_5/SiO_2$ catalyst.

For the Ni_xP_y/SiO_2 catalyst prepared from an oxidic precursor with P/Ni = 2.0, the XRD pattern exhibits peaks in addition to those for Ni_2P. The peaks for the crystalline impurity ($2\theta = 21.2°$, 25.6°, 26.7°, 28.4°, 30.0°, 31.6°, 35.1°, 38.2°, and 43.5°) are consistent with the presence of P_2O_5 (card no. 05-0318 [20]) and P_4O_7 (card no. 38-0932 [20]) on the silica support. Reference to Fig. 1 reveals that P is lost from the Ni_xP_y/SiO_2 catalysts only after phase-pure Ni_2P is formed on the silica support ($P/Ni \geqslant 0.8$). However, not all of the excess P is volatilized; instead some remains on the support as P_xO_y compounds.

Using the Scherrer equation [21], we calculated average crystallite sizes of 15 and 22 nm for the 30 wt% $Ni_{12}P_5/SiO_2$ and Ni_2P/SiO_2 catalysts, respectively. For these calculations, the full width at half-maximum (FWHM) of the {111} reflection at 40.8° for Ni_2P and the {312} reflection at 49.0° for $Ni_{12}P_5$ were used. TEM images of a 30 wt% $Ni_{12}P_5/SiO_2$ catalyst are shown in Fig. 3. The low-resolution TEM image (Fig. 3a) reveals that the $Ni_{12}P_5$ particle sizes range up to approximately 30 nm. The high-resolution image of a silica-supported $Ni_{12}P_5$ particle (Fig. 3b) indicates that $Ni_{12}P_5$ adopts a globular morphology on the silica support. The $Ni_{12}P_5$ particle has a diameter of 17 nm, and the indicated *d*-spacing is consistent with the {310} crystallographic plane of $Ni_{12}P_5$, as determined by comparison with the JCPDS powder diffraction file (card no. 22-1190 [20]). Low- and high-resolution images of a 25 wt% Ni_2P/SiO_2 catalyst were published previously [13]. After synthesis, the Ni_xP_y/SiO_2 catalysts were subjected to a flow of a 1 mol% O_2/He mixture at room temperature, so that a thin oxide layer formed on the outer surfaces of the particles, to prevent deep oxidation of the catalysts upon air exposure. The high-resolution TEM image displayed in Fig. 4 shows evidence of the passivation layer on a Ni_2P particle in a 30 wt% Ni_2P/SiO_2 catalyst. A light gray band with a thickness of approximately 2 nm can be seen to extend around the external edge of the Ni_2P particle.

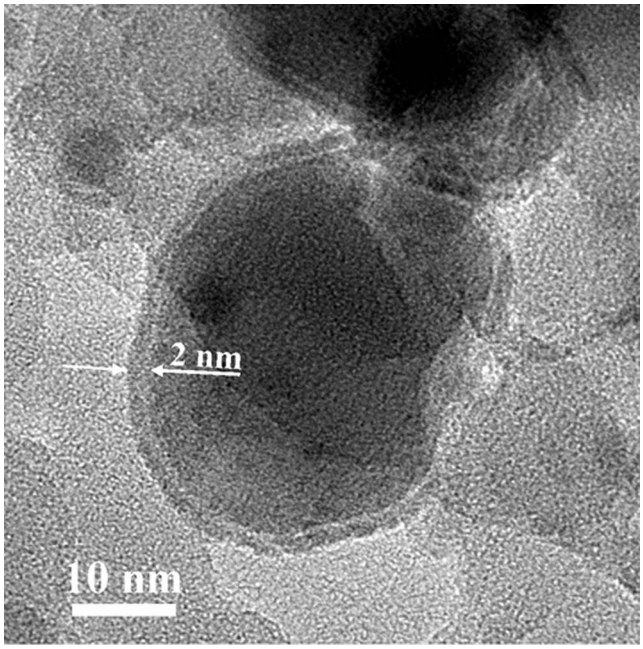

Fig. 4. High resolution TEM micrograph of a 25 wt% Ni_2P/SiO_2 catalyst.

The elemental compositions of the Ni_xP_y/Al_2O_3 catalysts are listed in Table 2, and the P/Ni molar ratios of the oxidic precursors and the Ni_xP_y/Al_2O_3 catalysts are plotted against one another in Fig. 1. For Ni_xP_y/Al_2O_3 catalysts prepared from oxidic precursors with P/Ni > 1.5, some P is lost from

Table 2
Physiochemical data for alumina-supported Ni_2P catalysts

Oxidic precursor molar ratio (P/Ni)	XRD phase(s)	Bulk composition	Surface composition	BET surface area (m^2/g)	Chemisorption capacity ($\mu mol_{O_2}/g$)	HDS activity[a] ($nmol_{Th}/(g_{cat}\ s)$)	HDS TOF[a] (s^{-1})
0.5	$Ni_{12}P_5$	$Ni_{1.88}P_{1.00}$	$Ni_{2.32}P_{1.00}$	66	123	166	0.0014
0.8	$Ni_{12}P_5$	$Ni_{1.23}P_{1.00}$	–	62	47	188	0.0039
1.0	$Ni_{12}P_5$, Ni_2P	$Ni_{1.03}P_{1.00}$	–	63	85	307	0.0036
1.5	$Ni_{12}P_5$, Ni_2P	$Ni_{0.66}P_{1.00}$	–	61	60	438	0.0073
2.0	Ni_2P	$Ni_{0.57}P_{1.00}$	$Ni_{0.25}P_{1.00}$	62	89	1020	0.012
2.5	Ni_2P	$Ni_{0.47}P_{1.00}$	–	53	54	396	0.0073

[a] After 48 h on-stream.

the catalysts during TPR, but all of the catalysts contain P in excess of that expected from the stoichiometry of Ni_2P. XRD patterns for the Ni_xP_y/Al_2O_3 catalysts and for unsupported Ni_2P and a reference pattern for $Ni_{12}P_5$ are shown in Fig. 5. The XRD patterns for the Ni_xP_y/Al_2O_3 catalysts show peaks associated with the γ-Al_2O_3 support ($2\theta = 32.5°$, 36.6°, 39.5°, 45.6°, and 67.1°) that are consistent with a reference pattern from the JCPDS powder diffraction file (card no. 02-1420 [20]). Excluding the peaks for γ-Al_2O_3, the XRD pattern for the Ni_xP_y/Al_2O_3 catalyst with a molar ratio P/Ni = 0.5 in the oxidic precursor shows only the peaks observed in the $Ni_{12}P_5$ reference pattern. Henceforth, this catalyst (P/Ni = 0.5) will be referred to as $Ni_{12}P_5/Al_2O_3$. The elemental composition of the $Ni_{12}P_5/Al_2O_3$ catalyst was determined to be $Ni_{1.88}P_{1.00}$, which is quite P-rich compared with the composition of $Ni_{12}P_5$ ($Ni_{2.4}P_{1.0}$). The only apparent peaks in the XRD pattern for the Ni_xP_y/Al_2O_3 catalyst prepared from an oxidic precursor with P/Ni = 0.8 are those for $Ni_{12}P_5$, whereas the catalysts prepared from precursors with P/Ni = 1.0 and 1.5 exhibit peaks for both $Ni_{12}P_5$ and Ni_2P. Phase-pure Ni_2P on the alumina support was successfully prepared from an oxidic precursor with a molar ratio P/Ni = 2.0. Henceforth, this catalyst will be referred to as Ni_2P/Al_2O_3. The elemental composition of the Ni_2P/Al_2O_3 catalyst was determined to be $Ni_{0.57}P_{1.00}$, which is very P-rich compared with the composition expected from the stoichiometry of Ni_2P. As the molar ratio in the oxidic precursors is increased to P/Ni = 2.5, Ni_2P is the only crystalline phase observed, but the peaks in the XRD pattern are substantially smaller than those for the Ni_2P/Al_2O_3 catalyst (P/Ni = 2.0). Similar to the silica-supported catalysts, reference to Fig. 1 reveals that P is lost from Ni_xP_y/Al_2O_3 catalysts only after phase-pure Ni_2P is formed on the alumina support ($P/Ni \geqslant 2.0$).

Average crystallite sizes of 11 and 15 nm were calculated for the 20 wt% $Ni_{12}P_5/Al_2O_3$ and Ni_2P/Al_2O_3 catalysts, respectively, with the use of the Scherrer equation and the same reflections as were used for the silica-supported catalysts. TEM images of the 20 wt% Ni_2P/Al_2O_3 and $Ni_{12}P_5/Al_2O_3$ catalysts (see Supplementary Information) reveal that the Ni phosphide particle sizes range up to approximately 30 nm for the Ni_2P/Al_2O_3 catalyst, but up to only about 16 nm for the $Ni_{12}P_5/Al_2O_3$ catalyst. The high-resolution images reveal that the alumina-supported Ni_2P and $Ni_{12}P_5$ particles adopt globular morphologies.

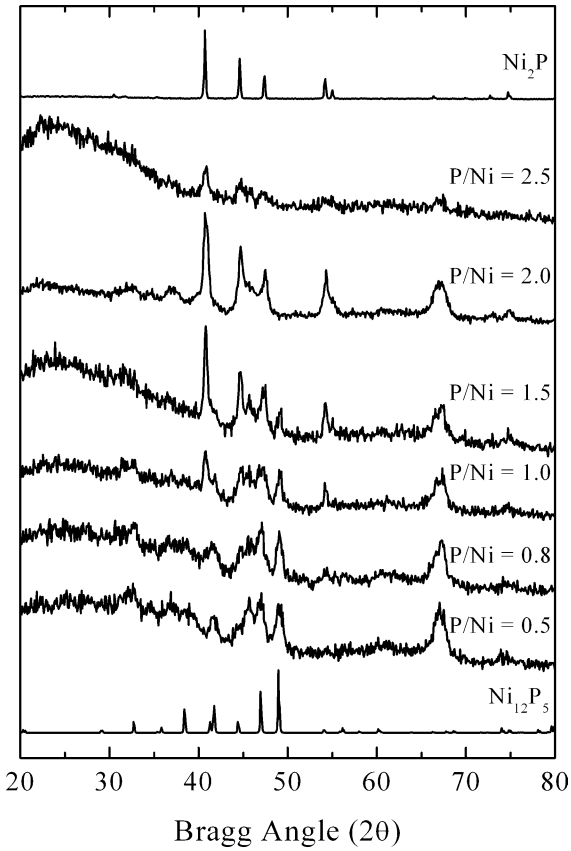

Fig. 5. XRD patterns for Ni_xP_y/Al_2O_3 catalysts with different P/Ni molar ratios in their oxidic precursors.

S analysis of silica- and alumina-supported Ni_2P and $Ni_{12}P_5$ catalysts was carried out after treatment at 650 K in a H_2S/H_2 mixture and subsequent passivation. The data for these measurements are given in Supplementary Information. If it is assumed that no P (or Ni) is lost from the catalysts during the H_2S/H_2 treatments and that the S is associated only with the Ni phosphide particles, then the composition of the phosphosulfide phases (NiP_xS_y) can be calculated. For the Ni_2P/SiO_2 and Ni_2P/Al_2O_3 catalysts, particle compositions of $Ni_{2.0}P_{1.0}S_{0.017}$ and $Ni_{2.0}P_{1.0}S_{0.050}$, respectively, can be determined. For the $Ni_{12}P_5/SiO_2$ and $Ni_{12}P_5/Al_2O_3$ catalysts, particle compositions of $Ni_{2.4}P_{1.0}S_{0.24}$ and $Ni_{2.4}P_{1.0}S_{0.25}$, respectively, can be calculated. Clearly, the more Ni-rich $Ni_{12}P_5$ phase incorporates substantially more

Table 3
Physiochemical data for sulfide catalysts

Catalyst	BET surface area (m^2/g)	Chemisorption capacity ($\mu mol_{O_2}/g$)	HDS activity[a] ($nmol_{Th}/(g_{cat}\ s)$)	HDS TOF[a] (s^{-1})
Sulf. Ni/SiO_2	113	72	136	0.0019
Sulf. Mo/SiO_2	92	18	232	0.013
Sulf. $Ni–Mo/SiO_2$	96	23	826	–
Sulf. Ni/Al_2O_3	81	317	379	0.0012
Sulf. Mo/Al_2O_3	58	54	782	0.014
Sulf. $Ni–Mo/Al_2O_3$	55	21	2190	–

[a] After 48 h on-stream.

sulfur as a result of treatment in H_2S/H_2 at 650 K than does Ni_2P. Using energy-dispersive X-ray analysis (EDAX), Korányi [14] detected no sulfur in unsupported Ni_2P sulfided in 10 mol% H_2S/H_2 at 673 K, and temperature-programmed sulfidation of Ni_2P showed insignificant uptake of H_2S at temperatures up to 1073 K. However, XPS showed some sulfur present at the surface of the sulfided Ni_2P [14]. After 300 h on stream in a mixed feed containing 3000 ppm dibenzothiophene, Oyama et al. [15] determined the elemental composition of a 24.4 wt% Ni_2P/SiO_2 catalyst to be $Ni_{2.0}P_{1.2}S_{0.060}$, consistent with the low S content reported here for a sulfided Ni_2P/SiO_2 catalyst.

3.1.2. BET surface area and O_2 chemisorption

The BET surface areas and O_2 chemisorption capacities for the Ni_xP_y/SiO_2 and Ni_xP_y/Al_2O_3 catalysts and for sulfided Ni/SiO_2, Ni/Al_2O_3, $Ni–Mo/SiO_2$, and $Ni–Mo/Al_2O_3$ ($Ni/Mo = 0.5$) catalysts are listed in Tables 1–3. For the Ni_xP_y/SiO_2 and Ni_xP_y/Al_2O_3 catalysts, the BET surface areas and O_2 chemisorption capacities generally decrease with increasing P content of the catalysts.

3.1.3. X-ray photoelectron spectroscopy

The XPS spectra in the Ni(2p) and P(2p) regions for 30 wt% Ni_2P/SiO_2 and $Ni_{12}P_5/SiO_2$ catalysts are shown in Fig. 6, and the spectra for 20 wt% Ni_2P/Al_2O_3 and $Ni_{12}P_5/Al_2O_3$ catalysts are shown in Fig. 7. The peaks in the XPS spectrum for the Ni_2P/SiO_2 catalyst have been assigned previously [13]. The peaks at 857.2 and 134.3 eV are assigned to Ni^{2+} and P^{5+} species, respectively, in the passivation layer formed on the Ni_2P particles following synthesis. The peaks observed at 853.5 and 129.5 eV are assigned to reduced Ni and P species, respectively. These binding energies indicate that the Ni in Ni_2P has a partial positive charge (δ^+), where $0 < \delta < 2$, whereas the P has a partial negative charge (δ^-), where $0 < \delta < 1$. The XPS spectrum for the $Ni_{12}P_5/SiO_2$ catalyst is similar to that for the Ni_2P/SiO_2 catalyst in most regards, but with some important differences. Two peaks are apparent in the Ni($2p_{3/2}$) region at 853.0 and 856.8 eV, which are assigned to $Ni^{\delta+}$ and Ni^{2+} species, respectively. The magnitude of δ must be quite small, as the Ni($2p_{3/2}$) binding energy of 853.0 eV is close to that of Ni metal (852.5–852.9 eV [22]). This binding energy is somewhat lower than that observed for Ni in the Ni_2P/SiO_2 catalyst, suggesting less transfer of electron density from Ni to P in $Ni_{12}P_5$. The peak intensities for the reduced and oxidized Ni species in the XPS spectrum for the $Ni_{12}P_5/SiO_2$ catalyst are also reversed from those for the

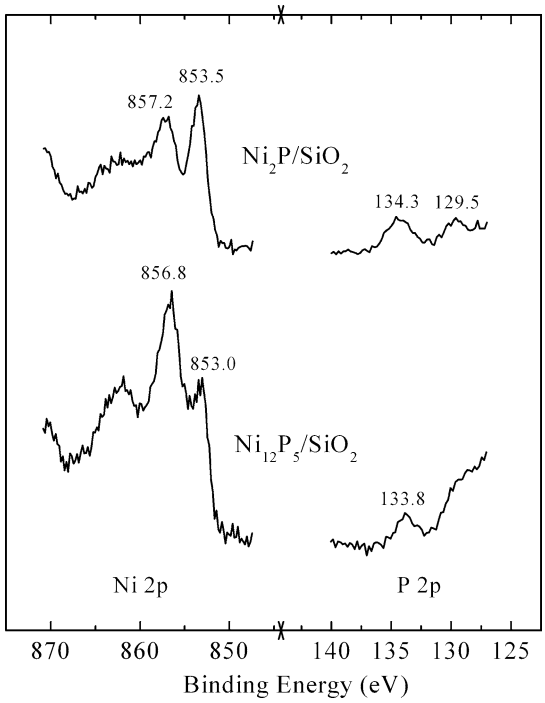

Fig. 6. XPS spectra in the Ni(2p) and P(2p) regions for 30 wt% Ni_2P/SiO_2 and $Ni_{12}P_5/SiO_2$ catalysts.

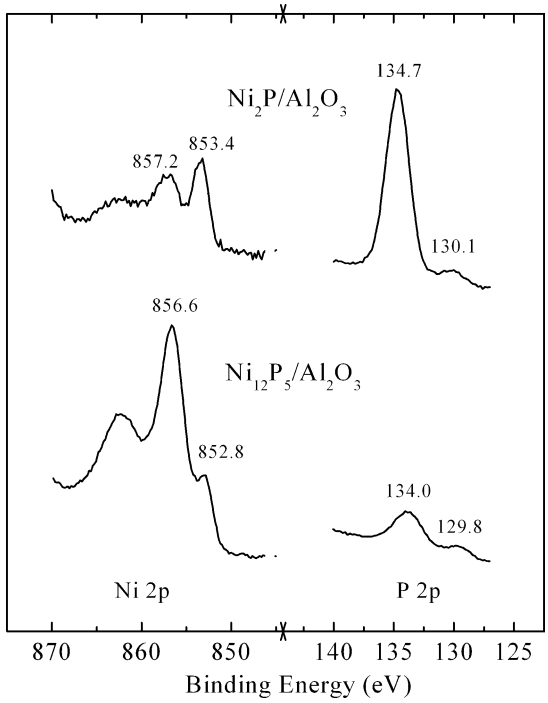

Fig. 7. XPS spectra in the Ni(2p) and P(2p) regions for 20 wt% Ni_2P/Al_2O_3 and $Ni_{12}P_5/Al_2O_3$ catalysts.

Ni_2P/SiO_2 catalyst, suggesting that there is a thicker passivation layer on the surface of the $Ni_{12}P_5/SiO_2$ catalyst. For this reason, the satellite peak at 862.0 eV, which is associated with Ni^{2+} species [23,24], is more pronounced for the $Ni_{12}P_5/SiO_2$ catalyst than for the Ni_2P/SiO_2 catalyst. In the P(2p) region, a peak at 133.8 eV is assigned to P^{5+} species in the passivation layer, and a weak shoulder at ~ 129.5 eV is assigned to $P^{\delta-}$ species, where $0 < \delta < 1$.

The XPS spectra for 20 wt% Ni_2P/Al_2O_3 and $Ni_{12}P_5/Al_2O_3$ catalysts (Fig. 7) generally mirror those for the silica-supported catalysts. The P(2p) region shows one significant difference: the XPS spectrum of the Ni_2P/Al_2O_3 catalyst has a very intense peak at 134.7 eV that is consistent with the binding energy of P in $AlPO_4$ molecular sieves (134.6–134.8 eV [25]). Some of the phosphorus impregnated onto the γ-Al_2O_3 in the form of $NH_4H_2PO_4$ is apparently reacting with the support to form $AlPO_4$ at the surface of the catalyst. This likely explains why a large excess of P ($P/Ni = 2.0$) is necessary in the oxidic precursor so that phase-pure Ni_2P can be prepared on γ-Al_2O_3. A slight excess of P ($P/Ni = 0.5$) was needed to prepare phase-pure $Ni_{12}P_5$ on γ-Al_2O_3, which may reflect that some P has reacted with the support in this catalyst to form $AlPO_4$ as well. Although the $P(2p_{3/2})$ binding energy (134.0 eV) for $Ni_{12}P_5/Al_2O_3$ catalyst is below that of $AlPO_4$, comparison of the P(2p) regions for the $Ni_{12}P_5$ catalysts (Figs. 6 and 7) reveals a substantially larger peak at ~ 134.0 eV for $Ni_{12}P_5$ supported on alumina than on silica. The surface Ni and P concentrations for the silica- and alumina-supported Ni_2P and $Ni_{12}P_5$ catalysts are listed in Tables 1 and 2.

3.1.4. Infrared spectroscopy of adsorbed CO

IR spectra for adsorbed CO on silica- and alumina-supported Ni, $Ni_{12}P_5$, and Ni_2P catalysts were acquired before and after exposure to 5.0 Torr CO. The IR spectra (not shown; acquired before CO exposure) in the ν_{OH} region show no evidence for P–OH species on the $Ni_{12}P_5/SiO_2$ and Ni_2P/SiO_2 catalysts, whereas a peak is apparent at 3676 cm^{-1} in the IR spectra of the $Ni_{12}P_5/Al_2O_3$ and Ni_2P/Al_2O_3 catalysts. This peak, which is slightly larger for the Ni_2P/Al_2O_3 catalyst, is assigned to the ν_{OH} mode of P–OH species [26]. The IR spectra for adsorbed CO on Ni/SiO_2 and Ni_2P/SiO_2 catalysts (Fig. 8) have recently been discussed elsewhere [16]. For the reduced Ni/SiO_2 catalyst, the intense ν_{CO} absorbance at 2074 cm^{-1} is assigned to CO terminally bonded to Ni^0 sites, and the two weak ν_{CO} absorbances at 1977 and 1915 cm^{-1} are assigned to CO adsorbed to Ni^0 bridge sites. A shoulder on the intense ν_{CO} absorbance at 2074 cm^{-1} is observed at 2056 cm^{-1} and is assigned to nickel tetracarbonyl ($Ni(CO)_4$) species formed upon CO adsorption.

The IR spectrum of adsorbed CO on the Ni/Al_2O_3 catalyst (Fig. 9) agrees well with IR spectra previously reported by others [27,28]. The peak position of the intense ν_{CO} absorbance at 2090 cm^{-1} is assigned to linearly bonded CO on Ni^0 sites [27,28]. The weak ν_{CO} absorbance at 2153 cm^{-1}

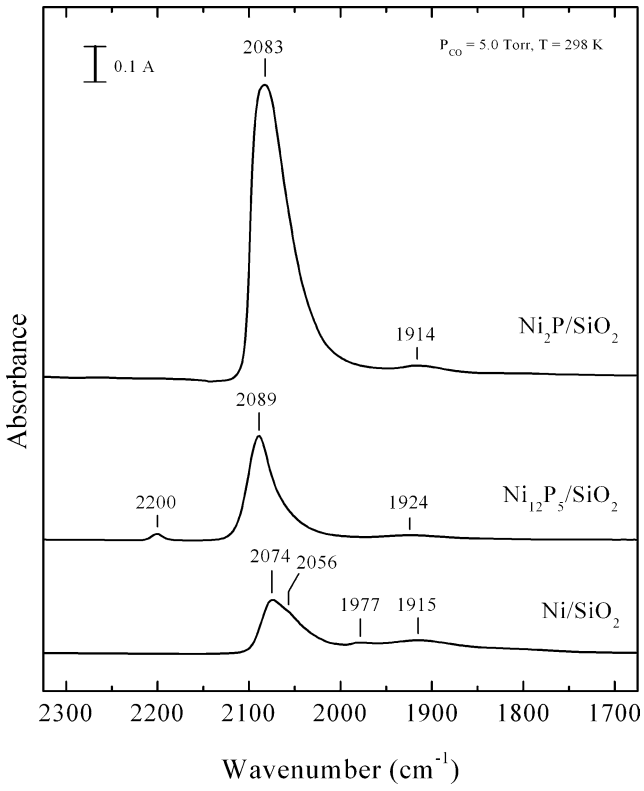

Fig. 8. Infrared spectra of adsorbed CO on reduced 20 wt% Ni/SiO_2, $Ni_{12}P_5/SiO_2$, and Ni_2P/SiO_2 catalysts.

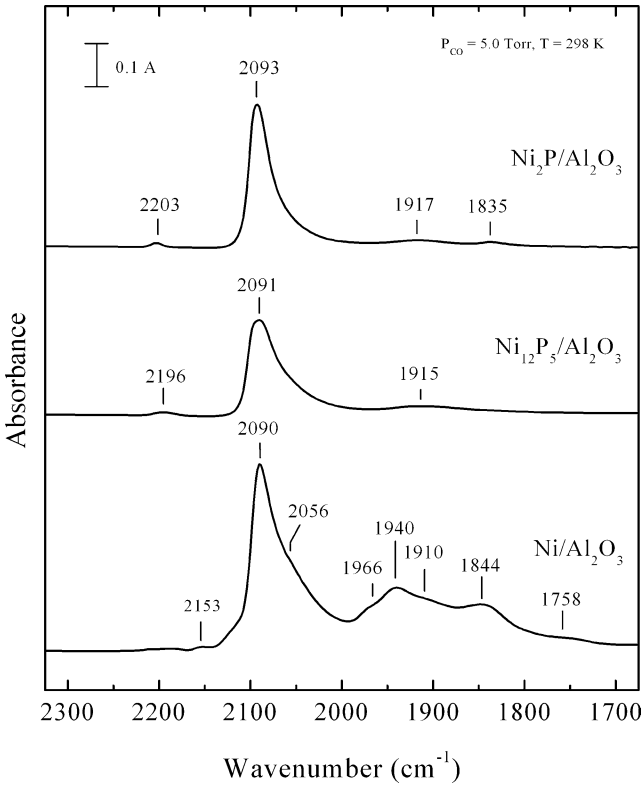

Fig. 9. Infrared spectra of adsorbed CO on reduced 20 wt% Ni/Al_2O_3, $Ni_{12}P_5/Al_2O_3$, and Ni_2P/Al_2O_3 catalysts.

Table 4
Infrared data for reduced and phosphide catalysts

Catalyst	ν_{CO}[a] (cm^{-1})	Relative CO site densities[a,b]
Ni/SiO_2	2074	0.87
Ni/Al_2O_3	2089	2.35
Ni_2P/SiO_2	2083	3.41
Ni_2P/Al_2O_3	2093	1.26
$Ni_{12}P_5/SiO_2$	2089	1.93
$Ni_{12}P_5/Al_2O_3$	2091	1.96

[a] For CO adsorbed on Ni atop sites only at 298 K.
[b] Integrated absorbance/mg catalyst.

is assigned to CO terminally adsorbed to an oxidized Ni site. The CO stretching vibrations observed at 1844, 1910, 1940, and 1966 cm^{-1} are assigned to CO adsorption on two-fold Ni^0 bridge sites [29–31]. The weak ν_{CO} absorbance at 1758 cm^{-1} has not been assigned. Similar to the Ni/SiO_2 catalyst, a shoulder at $\sim$ 2056 cm^{-1} is assigned to adsorbed $Ni(CO)_4$ on the catalyst surface. The peak positions for terminally bonded CO species and relative CO site densities are summarized in Table 4.

Substantial differences are observed in the IR spectra of adsorbed CO on the silica- and alumina-supported Ni catalysts upon incorporation of P to form $Ni_{12}P_5$ and Ni_2P phases (Figs. 8 and 9). CO adsorption on bridge sites and formation of $Ni(CO)_4$ are suppressed for the Ni phosphide catalysts, and the peak positions of the ν_{CO} absorbance associated with linearly bonded CO shift to higher wavenumbers. The ν_{CO} absorbance for CO adsorbed on atop Ni sites is centered at 2089 cm^{-1} for the $Ni_{12}P_5/SiO_2$ catalyst and at 2091 cm^{-1} for the $Ni_{12}P_5/Al_2O_3$ catalyst. For the Ni_2P/SiO_2 and Ni_2P/Al_2O_3 catalysts, this ν_{CO} absorbance is located at 2083 and 2093 cm^{-1}, respectively. It is unclear why the peak position of the ν_{CO} absorbance for linearly bonded CO on the Ni_2P/SiO_2 catalyst lies between the values for the Ni/SiO_2 and $Ni_{12}P_5/SiO_2$ catalysts. The heating characteristics vary slightly from sample to sample in our IR system, which may influence the extent of reduction of the thin oxide layer on the surface of silica-supported Ni_xP_y particles. As reported previously, the position of the ν_{CO} absorbance for CO adsorbed atop Ni sites of Ni_2P/SiO_2 catalysts was sensitive to the temperature and hydrogen pressure used for the reduction pretreatment [16]. A very weak ν_{CO} absorbance feature is observed at 2196–2203 cm^{-1} for the $Ni_{12}P_5/SiO_2$, $Ni_{12}P_5/Al_2O_3$, and Ni_2P/Al_2O_3 catalysts; a similar absorbance feature has also been observed for a Ni_2P/SiO_2 catalyst in 5.0 Torr CO at 150 K and a Ni_2P/SiO_2 catalyst reduced under milder conditions [16]. This ν_{CO} absorbance feature has recently been assigned to a surface-bonded P=C=O species [16]. A slight increase in the intensity of the IR absorbance at $\sim$ 2200 cm^{-1} is observed with increasing P content for the $Ni_{12}P_5/Al_2O_3$ and Ni_2P/Al_2O_3 catalysts, but the opposite trend is observed for the $Ni_{12}P_5/SiO_2$ and Ni_2P/SiO_2 catalysts. Given the sensitivity of the $\sim$ 2200 cm^{-1} absorbance band to reduction conditions [16] and the slight variations of the heating characteristics of samples in our IR system, we do not think it is prudent to try to correlate the small changes in the intensity of this band with the P content of the catalysts.

Infrared spectra were also acquired for adsorbed CO on silica- and alumina-supported $Ni_{12}P_5$ and Ni_2P catalysts after a sulfidation pretreatment at 650 K. As described previously, sulfidation of a 20 wt% Ni_2P/SiO_2 catalyst resulted in a decrease in the quantity of adsorbed CO and shifted the ν_{CO} absorbance for CO adsorbed on atop Ni sites from 2083 to 2093 cm^{-1}. These results indicate that some S is incorporated into or adsorbed onto Ni_2P/SiO_2 catalysts upon H_2S/H_2 pretreatment, blocking sites and withdrawing electron density from the Ni sites. The results for $Ni_{12}P_5/SiO_2$, $Ni_{12}P_5/Al_2O_3$, and Ni_2P/Al_2O_3 catalysts pretreated in H_2S/H_2 are consistent with those for the Ni_2P/SiO_2 catalyst; the quantity of adsorbed CO decreases and the ν_{CO} absorbance for CO adsorbed on atop Ni sites shifts to higher wavenumbers.

As indicated by the peak intensities and the relative CO site densities (Table 4), the amount of adsorbed CO is higher on the $Ni_{12}P_5/SiO_2$ catalyst relative to the Ni/SiO_2 catalyst, whereas a decrease is observed for the $Ni_{12}P_5/Al_2O_3$ and Ni/Al_2O_3 catalysts. These trends hold true for the Ni_2P/SiO_2 and Ni_2P/Al_2O_3 catalysts as well, with the Ni_2P/SiO_2 catalyst adsorbing the greatest amount of CO for the silica-supported catalysts, and the Ni_2P/Al_2O_3 catalyst adsorbing the least CO of the alumina-supported catalysts. Incorporation of P into the silica-supported catalysts apparently increases the dispersion of the Ni phase, whereas the large excess of P needed for the preparation of the alumina-supported Ni phosphide catalysts apparently blocks Ni sites on these catalysts.

3.1.5. Thiophene HDS activities

The thiophene HDS activities of the 30 wt% Ni_xP_y/SiO_2 and 20 wt% Ni_xP_y/Al_2O_3 catalysts after 48 h on stream are plotted in Fig. 10 as a function of the P/Ni molar ratios of the catalysts calculated from the bulk compositions listed in Tables 1 and 2. For both supports, the HDS activities of the Ni_xP_y catalysts depend strongly upon the composition of the oxidic precursors. Maxima of HDS activity are observed at compositions of $Ni_{1.64}P_{1.00}$ and $Ni_{0.57}P_{1.00}$ for the Ni_xP_y/SiO_2 and Ni_xP_y/Al_2O_3 catalysts, respectively. Reference to Tables 1 and 2 reveals that these compositions correspond to the oxidic precursors containing the lowest P contents that yield phase-pure Ni_2P on the oxide supports. For these optimized compositions, corresponding to the catalysts designated as Ni_2P/SiO_2 and Ni_2P/Al_2O_3, the silica-supported catalyst is 2.7 times more active than the alumina-supported catalyst after 48 h on stream. The presence of $Ni_{12}P_5$ in the silica- and alumina-supported Ni_xP_y catalysts has deleterious effects on the catalysts; $Ni_{12}P_5$ is substantially less active for thiophene HDS than is phase-pure Ni_2P on both supports. From the activity data summarized in Tables 1 and 2, it can be seen that the Ni_2P/SiO_2 catalyst is 4 times more active than the $Ni_{12}P_5/SiO_2$ catalyst

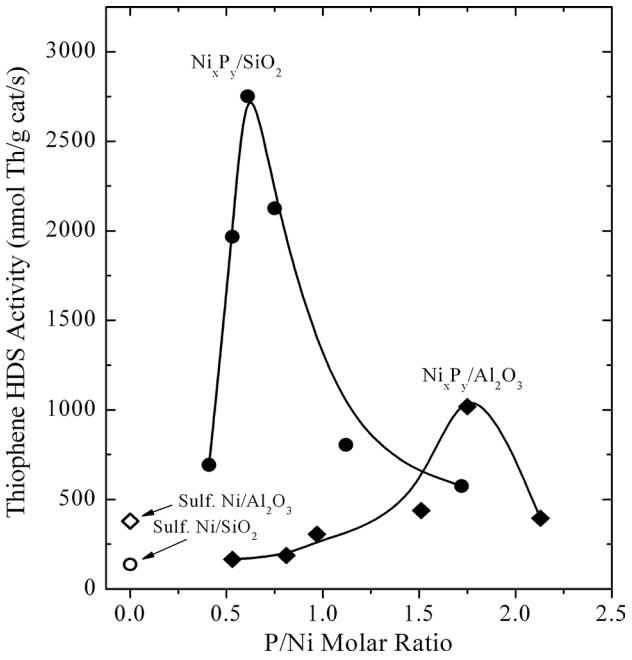

Fig. 10. Thiophene HDS activities (after 48 h on-stream) of 30 wt% Ni_xP_y/SiO_2 and 20 wt% Ni_xP_y/Al_2O_3 catalysts as a function of the composition (P/Ni molar ratio) of the catalysts.

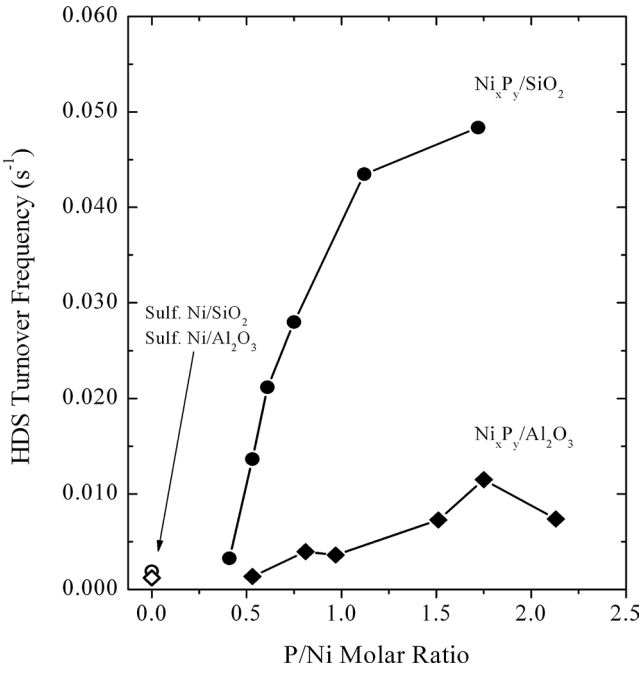

Fig. 11. Thiophene HDS turnover frequencies (after 48 h on-stream) of 30 wt% Ni_xP_y/SiO_2 and 20 wt% Ni_xP_y/Al_2O_3 catalysts as a function of the composition (P/Ni molar ratio) of the catalysts.

after 48 h on stream, and the Ni_2P/Al_2O_3 catalyst is 6 times more active than the $Ni_{12}P_5/Al_2O_3$ catalyst.

The turnover frequencies (TOFs) of the 30 wt% Ni_xP_y/SiO_2 and 20 wt% Ni_xP_y/Al_2O_3 catalysts, which we calculated by dividing the HDS activities after 48 h on stream by the O_2 chemisorption capacities, are plotted in Fig. 11 as a function of the P/Ni molar ratios of the catalysts. For the Ni_xP_y/SiO_2 catalysts, the TOFs increase sharply with increasing P content, whereas the Ni_xP_y/Al_2O_3 catalysts exhibit a much weaker trend of increasing TOF with P content.

The HDS activities and TOFs of the most active phosphide catalysts on the silica and alumina supports, Ni_2P/SiO_2 and Ni_2P/Al_2O_3, can be compared to those of sulfided Ni, Mo, and Ni–Mo (Ni/Mo = 0.5) on the two supports (see Tables 1–3). The 30 wt% Ni_2P/SiO_2 is more active than all of the sulfide catalysts, including 3.3 and 1.3 times more active than sulfided Ni–Mo/SiO_2 and Ni–Mo/Al_2O_3 catalysts, respectively, after 48 h on stream. The TOFs of the Ni_2P/SiO_2 and Ni_2P/Al_2O_3 catalysts are similar to or higher than those of the sulfided Ni and Mo catalysts.

4. Discussion

The synthesis utilized in this study to prepare Ni_xP_y/SiO_2 catalysts involved impregnation of the SiO_2 support with $Ni(NO_3)_2 \cdot 6H_2O$ followed by drying, calcination at 773 K, and subsequent impregnation with $NH_4H_2PO_4$. The precursors were not calcined after the phosphate impregnation. As reported previously [12,13], this synthesis method yields NiO on the silica support as detected by XRD and presumably adsorbed $NH_4H_2PO_4$ as depicted in Scheme 1. Time-resolved XRD showed that the reduction of an oxidic precursor with a molar ratio P/Ni = 0.8 proceeded sequentially to give Ni, $Ni_{12}P_5$, and ultimately Ni_2P on the silica support as the TPR proceeded (see Scheme 1) [12]. Prins and coworkers [7] have proposed a similar scheme for the reduction of oxidic precursors of Ni_xP_y/SiO_2 catalysts with molar ratios P/Ni = 0.5–0.65. The preparation procedure used in the current study, which has been described in detail in a previous publication [13], is different from that reported by the laboratories of Oyama [8,10] and Prins [7]. The syntheses used in the three groups vary in the sequence of impregnation and calcination steps and in the composition (P/Ni molar ratio) of the oxidic precursors. The synthesis developed in our laboratory yields Ni_2P/SiO_2 catalysts with smaller Ni_2P crystallites in comparison with catalysts prepared by the different methods but with similar loadings [13].

As the results of the current study indicate, the P/Ni molar ratio of the oxidic precursor is critical in determining the composition and properties of the Ni_xP_y/SiO_2 catalysts. For P/Ni < 0.8, there is insufficient P in the oxidic precursors to yield pure Ni_2P on the support, and the resulting catalysts contain $Ni_{12}P_5$. Reference to Fig. 1 shows that no P is lost from the oxidic precursors of Ni_xP_y/SiO_2 catalysts with P/Ni < 0.8. For these catalysts, P in the oxidic precursor is incorporated into the Ni phase, forming $Ni_{12}P_5$ or Ni_2P, or becomes associated with the silica support. To prepare phase-pure, silica-supported Ni_2P, excess P must be used in the catalyst precursor (P/Ni = 0.8). Some of this excess P is lost from the catalyst during TPR (presumably as PH_3), but the bulk composition of the Ni_2P/SiO_2 cata-

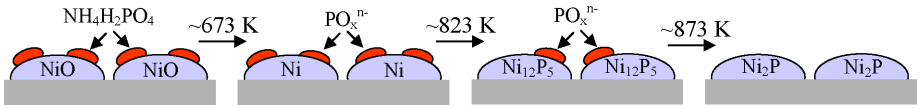

Scheme 1. Schematic representation of the silica-supported phases formed during TPR of the oxidic precursor of a Ni_2P/SiO_2 catalyst.

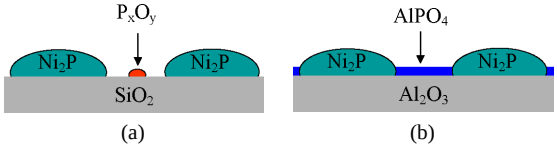

Scheme 2. Schematic representations of (a) Ni_2P/SiO_2 and (b) Ni_2P/Al_2O_3 catalysts.

lyst, $Ni_{1.64}P_{1.00}$, indicates that a substantial amount of the excess P remains on the catalyst. Using solid-state ^{31}P NMR spectroscopy, Prins and co-workers [7] observed no evidence for silicon phosphates on Ni_2P/SiO_2 catalysts, but did detect signals typical of phosphate species. As will be discussed shortly, studies by Oyama and co-workers [15] indicate that much of the excess P on the surface of Ni_2P/SiO_2 catalysts is lost during HDS. Similarly to Oyama et al. [15], we conclude that the excess P is associated with the silica support. For Ni_xP_y/SiO_2 catalysts prepared from oxidic precursors with molar ratios $P/Ni \geqslant 0.8$, phase-pure Ni_2P is formed on the silica and some P is lost from the catalyst during TPR, but increasing amounts of P remain associated with the support. For the Ni_xP_y/SiO_2 catalyst prepared from a precursor with $P/Ni = 2.0$, XRD peaks are assigned to P_2O_5 and P_4O_7 in addition to Ni_2P (see Fig. 2). Assuming that these same phases are formed in catalysts prepared from precursors with $0.8 \leqslant P/Ni < 2.0$ but that the crystallites are too small to be detected by XRD, the schematic representation of a freshly prepared Ni_2P/SiO_2 catalyst ($P/Ni = 0.8$) shown in Scheme 2a can be proposed. As the P/Ni molar ratio is increased above 0.8, the size of the P_xO_y particles increases. The BET surface areas and O_2 chemisorption capacities of the Ni_xP_y/SiO_2 catalysts decrease monotonically with increasing P content, indicating that the P_xO_y particles on the catalyst surface block access to adsorption sites.

Alumina-supported Ni_2P was not successfully prepared from oxidic precursors synthesized by the method described for silica-supported Ni_2P. Instead, a Ni_2P/Al_2O_3 catalyst was successfully synthesized from an oxidic precursor ($P/Ni = 2.0$) prepared by impregnation of γ-Al_2O_3 with a solution of $Ni(NO_3)_2 \cdot 6H_2O$ and $NH_4H_2PO_4$ followed by drying and calcination at 773 K. Complete reduction of the oxidic precursor to give alumina-supported Ni_2P required a maximum TPR temperature of 1123 K, 200 degrees higher than the maximum TPR temperature needed to prepare unsupported and silica-supported Ni_2P. Oyama and co-workers [1,32,33] observed similar differences in the preparation of MoP/SiO_2 and MoP/Al_2O_3 catalysts; the maximum TPR temperature needed for the alumina-supported MoP ($\geqslant$ 1123 K) was substantially higher than that needed for the silica-supported MoP (850 K). The higher temperatures needed to reduce the oxidic precursors of the alumina-supported phosphides are presumably due to the stronger interactions of the metals (Mo, Ni) and phosphate with γ-Al_2O_3 than with SiO_2. The stronger interaction of phosphate with γ-Al_2O_3 likely explains the need for a substantially higher P content in the oxidic precursor for the Ni_2P/Al_2O_3 catalyst ($P/Ni = 2.0$) than for the Ni_2P/SiO_2 catalyst ($P/Ni = 0.8$). As with the Ni_xP_y/SiO_2 catalysts, no P is lost from the Ni_xP_y/Al_2O_3 catalysts until phase-pure Ni_2P is synthesized on the support (see Fig. 1). Reference to the bulk compositions in Table 2 indicates that all of the Ni_xP_y/Al_2O_3 catalysts contain substantial excesses of P relative to the expected compositions of the Ni phosphide phases identified in the catalysts by XRD. Presumably this excess P is associated with the γ-Al_2O_3 support, and XPS (see Fig. 7) indicates that reaction has occurred to produce $AlPO_4$. A schematic representation of a freshly prepared Ni_2P/Al_2O_3 catalyst ($P/Ni = 2.0$) is shown in Scheme 2b. In contrast to the Ni_2P/SiO_2 catalyst, which required a smaller excess of P that interacts more weakly with the support (Scheme 2a), the schematic representation of the Ni_2P/Al_2O_3 catalyst (Scheme 2b) shows a layer of $AlPO_4$ covering the γ-Al_2O_3. A ν_{OH} absorbance at 3776 cm^{-1} in the IR spectra of the $Ni_{12}P_5/Al_2O_3$ and Ni_2P/Al_2O_3 catalysts that can be assigned to POH species supports this conclusion [34]. An $AlPO_4$ layer may also be present between the alumina and the Ni_2P particles.

A strong dependence of HDS activity on catalyst composition is observed for both the Ni_xP_y/SiO_2 and Ni_xP_y/Al_2O_3 catalysts, as shown in Fig. 10. For Ni_xP_y/SiO_2 catalysts prepared from oxidic precursors with compositions over the range $P/Ni = 0.4$–2.0, the catalyst with the highest activity ($P/Ni = 0.8$) was 4.8 times more active than the catalyst with the lowest activity ($P/Ni = 2.0$). The highest activity catalyst, designated Ni_2P/SiO_2, was also 20 times more active than a P-free sulfided Ni/SiO_2 catalyst with the same Ni loading. The optimal P/Ni molar ratio of the oxidic precursor ($P/Ni = 0.8$) is identified with the composition that contains just enough P to ensure formation of Ni_2P on the silica support. For $P/Ni < 0.8$, $Ni_{12}P_5$ is present on the silica, either alone or with Ni_2P, and this Ni phosphide is substantially less active for thiophene HDS than is Ni_2P. For $P/Ni > 0.8$, excess P remains on the catalyst surface, and the BET surface areas and O_2 chemisorption capacities of these catalysts decline quickly with increased P content. Oyama and co-workers [8] observed a similar dependence for the hydrodenitrogenation (HDN) of quinoline on the composition of the oxidic precursors of Ni_xP_y/SiO_2 catalysts, but observed only a very weak dependence for the HDS of dibenzothiophene. In addition to using a different

organosulfur compound, these authors utilized a mixed feed and prepared their oxidic precursors by a different method. The maximum in HDN activity was observed for oxidic precursors with molar ratios P/Ni = ∼ 2.0 [8], a much higher P content than for the optimal oxidic precursor (P/Ni = 0.8) examined in the current HDS study. Phase-pure Ni_2P was formed on the silica support for oxidic precursors with P/Ni ⩾ 1.0, but Oyama and co-workers [8] observed that higher P contents improved the dispersion of the supported Ni_2P. For an oxidic precursor with a molar ratio P/Ni = 3.0, the quinoline HDN activity fell precipitously, whereas the dibenzothiophene HDS activity dropped only slightly from its maximal value. Elemental analysis of the Ni and P contents of spent catalysts yielded compositions of $Ni_{1.75}P_{1.00}$ and $Ni_{1.33}P_{1.00}$ for Ni_xP_y/SiO_2 catalysts prepared from oxidic precursors with molar ratios P/Ni = 2.0 and 3.0, respectively [8]. During TPR of the oxidic precursors, evolution of PH_3 was observed for oxidic precursors with molar ratios P/Ni ⩾ 1.0. Korányi [14] observed a significant dependence of the thiophene HDS activity on precursor composition for Ni_xP_y/SiO_2 catalysts with molar ratios in the range P/Ni = 1.0–2.3; the highest HDS activities were observed for catalysts with P/Ni ⩾ 1.6 [14]. It is difficult to directly compare the results of the Korányi study directly with ours because of substantial differences in the catalyst synthesis.

A similar dependence of the HDS activity upon precursor composition is observed for the Ni_xP_y/Al_2O_3 catalysts, although the maximum of HDS activity is shifted to a more P-rich composition of P/Ni = 2.0. The most active Ni_xP_y/Al_2O_3 catalyst, designated Ni_2P/Al_2O_3, is 6.1 times more active than the catalyst with the lowest activity (P/Ni = 0.5) and is 2.7 times more active than a P-free sulfided Ni/Al_2O_3 catalyst. Consistent with the Ni_xP_y/SiO_2 catalysts, the optimal P/Ni molar ratio of the oxidic precursor is identified with the composition that contains just enough P to ensure formation of phase-pure Ni_2P on the support. This composition is more P-rich on alumina than on silica because more P becomes associated with the support for γ-Al_2O_3 instead of being available for incorporation in the Ni phosphide phase. For P/Ni < 2.0, $Ni_{12}P_5$ is present in the Ni_xP_y/Al_2O_3 catalysts and the HDS activity is lower than for the optimal composition.

Further insight into the properties of Ni_xP_y/SiO_2 and Ni_xP_y/Al_2O_3 catalysts is gained when the thiophene HDS TOFs of these catalysts are plotted as a function of their composition (see Fig. 11). The Ni_xP_y/SiO_2 catalysts exhibit a trend of steeply increasing TOFs with increased P content, whereas the Ni_xP_y/Al_2O_3 catalysts show a dramatically smaller increase in TOFs. Clearly, excess P yields catalysts with higher TOFs, even though the total number of sites decreases with increased P content (particularly for the silica-supported catalysts). Oyama and co-workers [8] observed that the P content of Ni_2P/SiO_2 catalysts decreases substantially during hydrotreating. Although excess P lowers HDS activity (on a per-gram basis) by blocking active sites, some of the excess P apparently serves the function of keeping the supported Ni_2P fully phosphided, thus facilitating high TOFs. If this is so, then one might expect a stronger effect for the silica-supported catalysts because the excess P is more strongly associated with alumina (forming $AlPO_4$) and is therefore less available to keep the Ni_2P fully phosphided. For the Ni_xP_y/SiO_2 catalysts in particular, there is a delicate balance between too much excess P, which blocks sites, and insufficient P to keep the Ni_2P fully phosphided.

As indicated by the TEM images (see Figs. 3 and 4 and Supplementary Information), $Ni_{12}P_5$ and Ni_2P particles adopt globular morphologies on both the SiO_2 and γ-Al_2O_3 supports, indicating no discernible dependence of the morphological properties of the supported particles on the Ni phosphide phase or the support type. The high-resolution image of a Ni_2P particle in Fig. 4 clearly shows a ∼ 2-nm-thick passivation layer at the outer edge of the particle. The XPS spectra (see Figs. 6 and 7) indicate that the passivation layer on the silica- and alumina-supported $Ni_{12}P_5$ and Ni_2P particles contains Ni^{2+} and PO_4^{3-} species, presumably in the form of NiO and $Ni_3(PO_4)_2$. The relative intensities of the Ni($2p_{3/2}$) peaks at 852.8–853.5 and 856.6–857.2 eV suggest that the passivation layer is thicker on the $Ni_{12}P_5$ particles than on the Ni_2P particles. The passivation layer is apparent in some high-resolution TEM images of the silica- and alumina-supported $Ni_{12}P_5$ catalysts, although it is less well defined than that shown for the silica-supported Ni_2P particle in Fig. 4.

The XPS spectra for the silica- and alumina-supported $Ni_{12}P_5$ and Ni_2P catalysts are generally similar, but the Ni($2p_{3/2}$) binding energies for reduced Ni species indicate less electron transfer from Ni to P for the $Ni_{12}P_5/SiO_2$ and $Ni_{12}P_5/Al_2O_3$ catalysts relative to the Ni_2P/SiO_2 and Ni_2P/Al_2O_3 catalysts. The surfaces of the $Ni_{12}P_5/SiO_2$ and $Ni_{12}P_5/Al_2O_3$ catalysts are substantially more Ni-rich than those of the Ni_2P/SiO_2 and Ni_2P/Al_2O_3 catalysts. The trend of the binding energies measured for the Ni phosphide catalysts is consistent with the XPS results of Korányi [14] that showed a shift of the Ni($2p_{3/2}$) binding energy from 853.1 eV for unsupported Ni_2P to 853.5 eV for unsupported Ni_5P_4. Taken together, the XPS results of the two studies indicate that as Ni phosphides become more P-rich ($Ni_{12}P_5 \rightarrow Ni_2P \rightarrow Ni_5P_4$), the Ni becomes increasingly electron poor; one should keep in mind, however, that the extent of the electron transfer from Ni to P is quite small in magnitude for these Ni phosphides. Using density function theory (DFT), Rodriguez et al. [12] recently calculated the magnitude of the positive charge on Ni in bulk Ni_2P to be 0.06. Based upon Knight shift measurements determined by ^{31}P NMR spectroscopy and consideration of the solid-state chemistry of Ni phosphides, Prins and co-workers [7] concluded that Ni_3P, $Ni_{12}P_5$, and Ni_2P exhibit metallic character. X-ray absorption spectroscopy (XAS) measurements and simulations by Oyama et al. [8,15] also indicate that $Ni_{12}P_5$ and Ni_2P have metallic properties. Consistent with our XPS measurements, however, the ^{31}P NMR and XAS results do indicate differences between the properties of $Ni_{12}P_5$ and Ni_2P. For

example, the XAS results show that the shortest Ni–Ni distances in $Ni_{12}P_5$ are shorter than those in Ni_2P [15]. This is in agreement with solid-state chemical results discussed by Prins and co-workers [7]; the shortest metal–metal distances in Ni_3P, $Ni_{12}P_5$, and Ni_2P are 0.244, 0.253, and 0.261 nm, respectively, whereas the shortest metal–metal distance in Ni metal is 0.249 nm. It would not be surprising if these and other structural and electronic differences are manifested in the catalytic properties of Ni phosphides with different stoichiometry.

Infrared spectra of adsorbed CO (see Figs. 8 and 9) show that P strongly affects the adsorption properties of $Ni_{12}P_5$ and Ni_2P on both supports relative to P-free Ni catalysts. CO adsorption on bridge sites is suppressed on the $Ni_{12}P_5$ and Ni_2P catalysts, as is formation of $Ni(CO)_4$ species, and the position of the terminally bonded ν_{CO} absorbance is shifted to higher wavenumbers, all relative to the P-free catalysts. This shift is likely due to the transfer of electron density from Ni to P in the phosphides, as observed by XPS. The IR spectra of the $Ni_{12}P_5/SiO_2$, $Ni_{12}P_5/Al_2O_3$, and Ni_2P/Al_2O_3 catalysts also exhibit a ν_{CO} absorbance at 2196–2203 cm^{-1} that is assigned to a phosphaketene-type species (P=C=O) formed by adsorption of CO on surface P atoms [16]. This species was first observed on a Ni_2P/SiO_2 catalyst, and the intensity of this absorbance was found to depend on the pretreatment conditions employed [16]. The results of the current and earlier studies indicate that surface P atoms are available for bonding with CO on the supported $Ni_{12}P_5$ and Ni_2P catalysts. It was recently suggested that direct interaction between thiophene and surface P atoms may play a role in the high reactivity of adsorbed thiophene on Ni_2P/SiO_2 catalysts [17].

The most profound difference between the $Ni_{12}P_5$ and Ni_2P catalysts, observed on both silica and alumina supports, was the S contents of the catalysts after pretreatment in an H_2S/H_2 mixture at 650 K. Silica- and alumina-supported Ni_2P incorporated relatively little S into its structure; particle compositions of $Ni_{2.0}P_{1.0}S_{0.017}$ and $Ni_{2.0}P_{1.0}S_{0.050}$ were calculated for the Ni_2P/SiO_2 and Ni_2P/Al_2O_3 catalysts, respectively. The molar amounts of S incorporated into the Ni_2P catalysts during H_2S/H_2 treatment are small (see Supplementary Information), less than the O_2 chemisorption capacities of the catalysts. In other words, the sulfur incorporated into Ni_2P/SiO_2 and Ni_2P/Al_2O_3 catalysts by an H_2S/H_2 pretreatment at 650 K, if restricted to surface adsorption only, is insufficient in quantity to block all of the adsorption sites titrated by O_2 chemisorption. Oyama et al. [15] determined the elemental composition of a 24.4 wt% Ni_2P/SiO_2 catalyst tested for 300 h on stream in a mixed feed to be $Ni_{1.0}P_{1.2}S_{0.060}$, also indicating that relatively small amounts of S are incorporated into supported Ni_2P catalysts under sulfiding conditions. Interestingly, we reported earlier that a 20 wt% Ni_2P/SiO_2 catalyst pretreated in H_2S/H_2 at 650 K was ∼ 10% more active for thiophene HDS than was a sample of this same catalyst reduced at 650 K in H_2 [13]. The O_2 chemisorption capacities for a *reduced* 20 wt% Ni_2P/SiO_2 catalyst (124 μmol/g) [13] and a *sulfided* 20 wt% Ni_2P/SiO_2 catalyst (126 μmol/g) [17] were determined to be identical within the error of the measurements. It is important to note that for the O_2 chemisorption measurement, the sulfided Ni_2P/SiO_2 catalyst was reduced in flowing H_2 following sulfidation. It may be, therefore, that a significant amount of the S incorporated into Ni_2P/SiO_2 catalysts upon H_2S/H_2 pretreatment is labile to hydrogenation and removal as H_2S, regenerating Ni sites. Alternatively, it may be that the incorporated S does not block Ni sites at the surface of the catalyst. Oyama and co-workers [8,11,15] and our laboratory [13,16,17] have concluded that the active catalytic phase is a mixed phosphosulfide (NiP_xS_y) phase, and the results presented here indicate that the S content of this phase is small.

The $Ni_{12}P_5/SiO_2$ and $Ni_{12}P_5/Al_2O_3$ catalysts incorporated 12 and 4.3 times more S into their structures than did the Ni_2P/SiO_2 and Ni_2P/Al_2O_3 catalysts, respectively (see Supplementary Information). Particle compositions of $Ni_{2.4}P_{1.0}S_{0.24}$ and $Ni_{2.4}P_{1.0}S_{0.25}$ can be calculated for the $Ni_{12}P_5/SiO_2$ and $Ni_{12}P_5/Al_2O_3$ catalysts, respectively. The molar amounts of S incorporated during H_2S/H_2 treatment are roughly twice the O_2 chemisorption capacities of the $Ni_{12}P_5$ catalysts, indicating that sulfidation of the supported $Ni_{12}P_5$ particles is more extensive than for the supported Ni_2P catalysts. It seems likely, therefore, that sulfidation of $Ni_{12}P_5/SiO_2$ and $Ni_{12}P_5/Al_2O_3$ catalysts under HDS reaction conditions is a critical factor for the low activity of these catalysts.

Given that γ-Al_2O_3 is the typical support for commercial hydrotreating catalysts [35], it is important to develop an understanding of the significantly lower thiophene HDS activities of the Ni_xP_y/Al_2O_3 catalysts compared with the Ni_xP_y/SiO_2 catalysts. For both series of catalysts, the highest HDS activities are observed for the catalysts containing the minimal P content in the oxidic precursors to give phase-pure Ni_2P on the supports (see Tables 1 and 2, and Fig. 10). The Ni_2P/SiO_2 catalyst ($P/Ni = 0.8$) is 2.7 times more active than the Ni_2P/Al_2O_3 catalyst ($P/Ni = 2.0$). There is no evidence in the physicochemical characterization results for the supported Ni_2P presented here that suggests different sites on the two catalysts. The Ni_2P particles adopt globular morphologies on both supports, indicating that there are no major differences in the crystal planes exposed. The Ni($2p_{3/2}$) binding energies measured for the reduced Ni species (853.4–853.5 eV) in the Ni_2P particles are similar on silica and alumina supports, whereas IR spectroscopy of adsorbed CO does suggest subtle differences in the electronic properties of surface Ni sites on the Ni_2P/SiO_2 and Ni_2P/Al_2O_3 catalysts. The terminally bonded ν_{CO} absorbance is located at 2083 cm^{-1} for the Ni_2P/SiO_2 catalyst and at 2093 cm^{-1} for the Ni_2P/Al_2O_3 catalyst, both pretreated in flowing H_2 at 650 K. This difference may be due to the influence of the support on the electronic properties of Ni sites of the Ni_2P particles. Recent IR spectral studies have shown a smooth variation of the ν_{CO} absorbance for adsorbed CO on metal sulfides supported on oxides with dif-

ferent acidities [36,37]. As the support acidity increased, the position of the ν_{CO} absorbance shifted to higher frequencies. It is unclear, however, how this electronic perturbation of the Ni_2P particles supported on γ-Al_2O_3 (relative to SiO_2) would affect thiophene HDS activity, but we expect that this influence would be small.

To understand the lower HDS activities of the Ni_xP_y/Al_2O_3 catalysts compared with Ni_xP_y/SiO_2 catalysts, it is important to consider the different interactions of P with SiO_2 and γ-Al_2O_3. Significantly more P must be added to the oxidic precursors of Ni_xP_y/Al_2O_3 catalysts than to those of Ni_xP_y/SiO_2 catalysts to prepare phase-pure Ni_2P on the supports (see Tables 1 and 2). It is expected that $AlPO_4$ forms in the oxidic precursors of the alumina-supported catalysts upon calcination, whereas it does not appear that silicon phosphates form in the silica-supported catalysts. The P contents of the Ni_xP_y/Al_2O_3 catalysts are quite high, ranging from 4.1 wt% (P/Ni = 0.5) to 12.4 wt% (P/Ni = 2.5), where the weight percentages correspond to the reduced catalysts and the molar ratios refer to the oxidic precursors. Studies published by others indicate that $AlPO_4$ is formed at the surface of γ-Al_2O_3 for P loadings greater than or equal to 4 wt% [34,38–42]. $AlPO_4$ is readily formed on γ-Al_2O_3 by reaction with phosphoric acid (H_3PO_4), but it is also formed via reaction with $NH_4H_2PO_4$ when used in high loadings. The $AlPO_4$ formed is often amorphous, so it is not surprising that no reflections associated with it are observed in the XRD patterns of the Ni_xP_y/Al_2O_3 catalysts (see Fig. 5). Evidence for the formation of $AlPO_4$ in the Ni_xP_y/Al_2O_3 catalysts comes from XPS (see Fig. 7); the P(2p) region for a Ni_2P/Al_2O_3 (P/Ni = 2.0) catalyst shows a large peak at a binding energy (134.7 eV) consistent with $AlPO_4$ formation. The restructuring of the alumina surface due to $AlPO_4$ formation is likely responsible for the low BET surfaces of the Ni_xP_y/Al_2O_3 catalysts and the poorer dispersion of the Ni phosphide phases. However, the lower HDS activities of the Ni_xP_y/Al_2O_3 catalysts compared with the Ni_xP_y/SiO_2 catalysts cannot be traced solely to poorer dispersion of Ni_2P on the alumina support. As discussed earlier, the HDS TOFs are substantially lower for the Ni_xP_y/Al_2O_3 catalysts than for the Ni_xP_y/SiO_2 catalysts, and we concluded that this may be due to excess P on the silica-supported catalysts being more available to keep the Ni_2P fully phosphided than on the alumina-supported catalysts.

5. Conclusions

The HDS properties of Ni_xP_y/SiO_2 and Ni_xP_y/Al_2O_3 catalysts prepared from oxidic precursors with a range of P/Ni molar ratios have been investigated. Oxidic precursors with molar ratios of P/Ni = 0.8 and 2.0 yielded catalysts containing phase-pure Ni_2P on the silica and alumina supports, respectively, and these catalysts have the highest HDS activities of the Ni_xP_y/SiO_2 and Ni_xP_y/Al_2O_3 catalysts. For P/Ni molar ratios lower than the optimal values, significant $Ni_{12}P_5$ impurities were present in the Ni_xP_y/SiO_2 and Ni_xP_y/Al_2O_3 catalysts, and these deleteriously affected the HDS properties of the catalysts. The low HDS activity of supported $Ni_{12}P_5$ is attributed to the incorporation of significant amounts of S into its structure under sulfiding conditions. For P/Ni molar ratios higher than the optimal values, excess P on the catalyst surfaces lowers the HDS activities of the Ni_xP_y/SiO_2 and Ni_xP_y/Al_2O_3 catalysts. Amorphous $AlPO_4$ is formed on all of the Ni_xP_y/Al_2O_3 catalysts because of the high P loadings used in the catalyst syntheses, and we believe this is responsible for the lower HDS activity of these catalysts relative to the Ni_xP_y/SiO_2 catalysts.

Acknowledgments

This research was supported by the National Science Foundation under grant number CHE-0101690 and the Camille and Henry Dreyfus Scholar/Fellow Program for Undergraduate Institutions. A portion (TEM, XPS) of the research described in this paper was performed in the Environmental Molecular Sciences Laboratory (EMSL), a national scientific user facility sponsored by the Department of Energy's Office of Biological and Environmental Research and located at Pacific Northwest National Laboratory. The authors acknowledge Kevin Nordby and ConocoPhillips (Ferndale refinery) for performing the sulfur analyses and Prof. S. Ted Oyama for helpful discussions.

Supplementary material

The online version of this article contains additional supplementary material.

Please visit DOI:10.1016/j.jcat.2005.01.020.

References

[1] P. Clark, X. Wang, S.T. Oyama, J. Catal. 207 (2002) 256.
[2] D.C. Phillips, S.J. Sawhill, R. Self, M.E. Bussell, J. Catal. 207 (2002) 266.
[3] V. Zuzaniuk, R. Prins, J. Catal. 219 (2003) 85.
[4] P. Clark, W. Li, S.T. Oyama, J. Catal. 200 (2001) 140.
[5] S.T. Oyama, P. Clark, X. Wang, T. Shido, Y. Iwasawa, S. Hayashi, J.M. Ramallo-Lopez, F.G. Requejo, J. Phys. Chem. B 106 (2002) 1913.
[6] W.R.A.M. Robinson, J.N.M. van Gestel, J. Catal. 161 (1996) 539.
[7] C. Stinner, Z. Tang, M. Haouas, T. Weber, R. Prins, J. Catal. 208 (2002) 456.
[8] S.T. Oyama, X. Wang, Y.-K. Lee, K. Bando, F.G. Requejo, J. Catal. 210 (2002) 207.
[9] S.T. Oyama, X. Wang, F.G. Requejo, T. Sato, Y. Yoshimura, J. Catal. 209 (2002) 1.
[10] X. Wang, P. Clark, S.T. Oyama, J. Catal. 208 (2002) 321.
[11] S.T. Oyama, J. Catal. 216 (2003) 343.
[12] J.A. Rodriguez, J.-Y. Kim, J.C. Hanson, S.J. Sawhill, M.E. Bussell, J. Phys. Chem. B 107 (2003) 6276.
[13] S.J. Sawhill, D.C. Phillips, M.E. Bussell, J. Catal. 215 (2003) 208.
[14] T. Korányi, Appl. Catal. A 239 (2003) 253.
[15] S.T. Oyama, X. Wang, Y.-K. Lee, W.-J. Chun, J. Catal. 221 (2004) 263.
[16] K.A. Layman, M.E. Bussell, J. Phys. Chem. B 108 (2004) 10930.

[17] K.A. Layman, M.E. Bussell, J. Phys. Chem. B 108 (2004) 15791.
[18] P.A. Aegerter, W.W.C. Quigley, G.J. Simpson, D.D. Ziegler, J.W. Logan, K.R. McCrea, S. Glazier, M.E. Bussell, J. Catal. 164 (1996) 109.
[19] A.L. Diaz, M.E. Bussell, J. Phys. Chem. 97 (1993) 470.
[20] JCPDS Powder Diffraction File International Centre for Diffraction Data, Swarthmore, PA, 2000.
[21] C. Suryanarayana, M.G. Norton, X-Ray Diffraction: A Practical Approach, Plenum Press, New York, 1998.
[22] D. Briggs, M.P. Seah (Eds.), Practical Surface Analysis by Auger and X-Ray Photoelectron Spectroscopy, Wiley, New York, 1983.
[23] A.N. Mansour, Surf. Sci. Spectra 3 (1994) 231.
[24] K.T. Ng, J. Phys. Chem. 80 (1976) 2094.
[25] S.L. Suib, A.M. Winiecki, A. Kostapapas, Langmuir 3 (1987) 483.
[26] J.M. Lewis, R.A. Kydd, J. Catal. 136 (1992) 478.
[27] C.E. O'Neill, D.J.C. Yates, J. Phys. Chem. 65 (1961) 901.
[28] M.L. Hair, Infrared Spectroscopy in Surface Chemistry, Dekker, New York, 1967.
[29] M. Nishijima, S. Masuda, Y. Sakisaka, M. Onchi, Surf. Sci. 107 (1981) 31.
[30] J.C. Campuzano, R.G. Greenler, Surf. Sci. 83 (1979) 301.
[31] W. Erley, H. Wagner, H. Ibach, Surf. Sci. 80 (1979) 612.
[32] S.T. Oyama, P. Clark, V.L.S. Teixiera da Silva, E.J. Lede, F.G. Requejo, J. Phys. Chem. B 105 (2001) 4961.
[33] P.A. Clark, S.T. Oyama, J. Catal. 218 (2003) 78.
[34] J.A.R. van Veen, P.A.J.M. Hendriks, R.R. Andréa, E.J.G.M. Romers, A.E. Wilson, J. Phys. Chem. 94 (1990) 5282.
[35] H. Topsøe, B. Clausen, F.E. Massoth, in: J.R. Anderson, M. Boudart (Eds.), Catalysis: Science and Technology, vol. 11, Springer, Berlin, 1996, p. 1.
[36] C.-D. Hédoire, C. Louis, A. Davidson, M. Breysse, F. Maugé, M. Vrinat, J. Catal. 220 (2003) 433.
[37] F. Maugé, G. Crépeau, A. Travert, T. Cseri, Prepr. Div. Fuel Chem. ACS 48 (2003) 131.
[38] M. McMillan, J.S. Brinen, G.L. Haller, J. Catal. 97 (1986) 243.
[39] P. Mangnus, J.A.R. van Veen, S. Eijsbouts, V.H.J. de Beer, L.A. Moulijn, Appl. Catal. 61 (1990) 99.
[40] O.H. Han, C.Y. Lin, G.L. Haller, Catal. Lett. 14 (1992) 1.
[41] O.H. Han, C.Y. Lin, N. Sustache, M. McMillan, D.J. Carruthers, K.W. Zilm, G.L. Haller, Appl. Catal. A 98 (1993) 195.
[42] E. Decanio, J. Edwards, T. Scalzo, D. Storm, J. Bruno, J. Catal. 132 (1991) 498.